Disentangling the role of chain conformation on the mechanics of polymer tethered particle materials

Jiarul Midya,[†] Yu Cang,[‡] Sergei A. Egorov,[¶] Krzysztof Matyjaszewski,[§] Michael R. Bockstaller,[‖] Arash Nikoubashman,[*,†] and George Fytas[*,‡]

Institute of Physics, Johannes Gutenberg University Mainz, Staudingerweg 7, 55128 Mainz, Germany, Max Planck Institute for Polymer Research, Ackermannweg 10, 55128, Mainz, Germany, Department of Chemistry, University of Virginia, McCormick Road, Charlottesville, VA 22904-4319, United States, Chemistry Department, Carnegie Mellon University, 4400 Forbes Ave., Pittsburgh, PA 15213, United States, and Department of Materials Science and Engineering, Carnegie Mellon University, 5000 Forbes Ave., Pittsburgh, PA 15213, United States

E-mail: anikouba@uni-mainz.de; fytas@mpip-mainz.mpg.de

[*]To whom correspondence should be addressed

[†]Institute of Physics, Johannes Gutenberg University Mainz, Staudingerweg 7, 55128 Mainz, Germany

[‡]Max Planck Institute for Polymer Research, Ackermannweg 10, 55128, Mainz, Germany

[¶]Department of Chemistry, University of Virginia, McCormick Road, Charlottesville, VA 22904-4319, United States

[§]Chemistry Department, Carnegie Mellon University, 4400 Forbes Ave., Pittsburgh, PA 15213, United States

[‖]Department of Materials Science and Engineering, Carnegie Mellon University, 5000 Forbes Ave., Pittsburgh, PA 15213, United States

Experimental Details

Materials: Particle brush synthesis was performed using surface-initiated atom transfer radical polymerization following a procedure described previously.[1] The final molar ratios of reaction components in a typical reaction were approximately $[\mathrm{Styrene}]_0 : [\mathrm{SiO_2 - Br}]_0 : [\mathrm{CuBr}]_0 : [\mathrm{CuBr_2}]_0 : [\mathrm{PMDETA}]_0$ of 2000 : 1 : 2.5 : 0.25 : 2.75 with a volume fraction of non-reactive solvents of 5.4% dimethylformamide and 40% anisole in a 100 mL flask. The polymerization was stopped by exposing the catalyst to oxygenated tetrahydrofuran after cooling under continuous stirring at approximately 1000 rpm. The final product was dialyzed against tetrahydrofuran and methanol until the copper (II) catalyst was removed as evidenced by disappearance of its characteristic color.

Styrene (St, Aldrich, 99%) was purified by passing through a basic alumina column before use. Copper (I) bromide was prepared by reduction of an aqueous solution of $CuBr_2$ with an aqueous solution of ascorbic acid. Copper (I) chloride was prepared by reduction of $CuCl_2$ aqueous solution using an aqueous solution of sodium sulfite. Both copper (I) halides were then sequentially filtered, washed with methanol, dried and stored under vacuum before use. Silica nanoparticles (SiO_2 NP), 30% solution in isopropanol, effective diameter, $d_{TEM} \approx 113$ nm, were donated by Nissan Chemical Corporation and used as received. 5−Hexen−1−ol (98%), $\alpha-$bromoisobutyryl bromide (98%), triethoxysilane (95%), ethyl 2−bromoisobutyrate (EBiB, 98%), 4, 4′-Dinonyl−2, 2′-bipyridine (dNbpy, 99%), N, N, N', N'', N''-pentamethyldiethylenetriamine (PMDETA, 99%), and anisole (99%) were purchased from Aldrich and used as received. All other chemicals and solvents were supplied by Aldrich and Acros Organics.

Table S1 gives an overview of the polystyrene (PS)-tethered silica materials used in the experiments.

Brillouin Light Scattering (BLS): Utilizing the photoelastic interactions between incident light and thermally activated phonons, BLS[3] records the spectra of inelastically

Table S1: Parameters of the PS-tethered silica particles. The volume fraction of PS ($\phi_{\rm PS}$) is determined by using different methods.[2] The mass density (ρ) is determined by using the relation $\rho = \rho_{\rm PS}\phi_{\rm PS} + \rho_{\rm silica}(1 - \phi_{\rm PS})$, where $\rho_{\rm PS} = 1.05\,\mathrm{g/cm^3}$ and $\rho_{\rm silica} = 1.85\,\mathrm{g/cm^3}$.

Sample ID	σ [nm^{-2}]	Degree of polymerization	$\phi_{\rm PS}$	ρ (g/cm^3)
DP100	0.61	130	0.48±0.04	1.47
DP1170	0.08	1170	0.50±0.02	1.45
DP530	0.30	530	0.56±0.02	1.40
DP1300	0.53	1300	0.86±0.04	1.16
DP400	0.61	400	0.70±0.03	1.29
DP600	0.56	630	0.78±0.03	1.23
DP1000	0.48	980	0.82±0.02	1.19
DP2480	0.39	2480	0.93±0.03	1.11

scattered light by phonons with wave vector $\mathbf{k}$ equal to scattering wave vector $\mathbf{q}$. The $\mathbf{q} = \mathbf{k}_{\rm i} - \mathbf{k}_{\rm s}$ along a specific direction could be selected by scattering geometry, with $\mathbf{k}_{\rm i}$ and $\mathbf{k}_{\rm s}$ being the wave vector of incident and scattering light respectively. For the periodic structure, the spectrum consists of a single doublet with a Doppler shift of $2\pi f = \pm c_{\rm l(t)} q$ in the low $\mathbf{q}$ regime, where $c_{\rm l(t)}$ is the effective medium sound velocity of longitudinal (transverse) phonons selected by input polarizer V(V) and output analyzer V(H). Therefore, the transmission geometry is employed in this work that allows $q = \frac{4\pi}{\lambda}\sin(\theta/2)$ varying at low values for which the systems appears homogeneous, where θ is the scattering angle and $\lambda = 532\,\mathrm{nm}$ is the wavelength of input light. The longitudinal (shear) modulus is computed as $M(G) = \rho c_{\rm l(t)}^2$ with ρ being the density of self-assembled films.

Simulation Model and Methods

Simulation Model Nanoparticles (NPs) are modeled as spherical clusters of Lennard-Jones (LJ) particles. Each LJ particle has unit diameter a and unit mass m. The NPs are considered as uniform spheres of unit reduced density. The resulting interaction between two NPs at distance r is given by the Hamaker potential[4,5]

$$U_{\mathrm{NN}}(r) = \begin{cases} -\frac{A_{\mathrm{NN}}}{6}\left[\frac{2R^2}{r^2-4R^2} + \frac{2R^2}{r^2} + \ln\left(\frac{r^2-4R^2}{r^2}\right)\right] + \frac{A_{\mathrm{NN}}}{37800}\frac{a^6}{r}\left[\frac{r^2-14rR+54R^2}{(r-2R)^7}\right. & \\ \left. + \frac{r^2+14rR+54R^2}{(r+2R)^7} - \frac{2(r^2-30R^2)}{r^7}\right] & \text{for } r \leq r_{\mathrm{c,NN}} \\ 0 & \text{for } r > r_{\mathrm{c,NN}} \end{cases} \tag{1}$$

where R is the radius of the NP, $r_{\mathrm{c,NN}}$ is the cut-off distance of the potential, and A_{NN} is the Hamaker constant which controls the strength of the potential. The grafted polymer chains are represented by the bead-spring Kremer-Grest model, where two monomers are interacting via the LJ potential[6]

$$U_{\mathrm{mm}}(r) = \begin{cases} \varepsilon\left[\left(\frac{a}{r}\right)^{12} - \left(\frac{a}{r}\right)^{6}\right] & \text{for } r \leq r_{\mathrm{c,mm}} \\ 0 & \text{for } r > r_{\mathrm{c,mm}} \end{cases} \tag{2}$$

where r is the distance between two monomers, $r_{\mathrm{c,mm}} = 3a$ is the cut-off distance of the potential, and ε is the strength of the potential. The monomers are bonded via the finitely extensible nonlinear elastic (FENE) potential[7,8]

$$U_{\mathrm{FENE}}(r) = -\frac{1}{2}\kappa r_0^2 \ln\left[1 - \left(\frac{r}{r_0}\right)^2\right]. \tag{3}$$

Here, r_0 is the maximum bond extension which is set to $r_0 = 1.5\,a$, and κ is the spring constant which is set to $\kappa = 30\varepsilon/a^2$. These values prevent unphysical bond crossing.

The polymers are grafted to the NPs by rigidly attaching the first polymer bead to the NP surface. These grafting points are randomly distributed on the NP surface. Then the remainder of the chains is fastened to those grafting beads (see the schematic representation given in Fig. S1). The interaction between a monomer and an NP at a distance r apart is

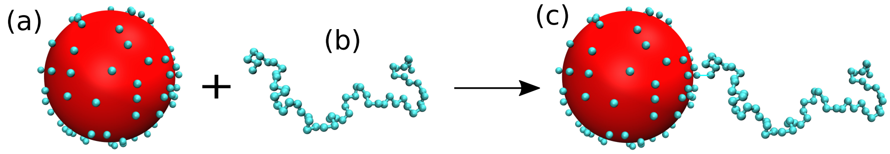

Figure S1: Schematic of (a) an NP with all the grafting beads, (b) a free polymer chain that will be grafted to the NP, and (c) the resulting NP with one grafted chain.

also described via the Hamaker potential[5]

$$U_{\mathrm{Nm}}(r) = \begin{cases} -\frac{2}{9}\frac{R^3 a^3 A_{\mathrm{Nm}}}{(R^2-r^2)^3}\left[1 - \frac{(5R^6+45R^4r^2+63R^2r^4+15r^6)a^6}{15(R^2-r^2)^6}\right] & \text{for } r \leq r_{\mathrm{c,Nm}} \\ 0 & \text{for } r > r_{\mathrm{c,Nm}} \end{cases} \tag{4}$$

where $r_{\mathrm{c,Nm}}$ is the cut-off distance of the potential, and A_{Nm} is the Hamaker constant between an NP and a monomer.

The experimental systems are mapped to our MD simulations in the following way. First, we calculate for all experimental systems the volume of an NP (V_{NP}) as well as the total volume of PS (V_{PS}) attached to it. To calculate V_{PS} we have used the mass density of PS ($\rho_{\mathrm{PS}} = 1.05\,\mathrm{g/cm^3}$) and the molar mass of a styrene monomer (104.1 g/mol).[9] Then, we have determined the volume ratio $W = V_{\mathrm{PS}}/V_{\mathrm{NP}}$ for all the experimental systems. In our simulations, the radius of the NPs is set to $R = 10\,a$ and we tuned the degree of polymerization in such a way that provides the same value of W as in the experiment. The number of grafting points on the NPs is chosen to match the grafting density of the experimental samples. In all our simulations, the cut-off distances are $r_{\mathrm{c,NN}} = 35\,a$ and $r_{\mathrm{c,Nm}} = 15\,a$. The value of the Hamaker constants for silica-silica and PS-PS interactions are 6.5×10^{-20} J and 7.25×10^{-20} J, respectively.[10] We determined the Hamaker constant for the silica-PS interaction from the geometric mean which gives 6.9×10^{-20} J. We converted these numbers to reduced units using a conversion factor $k_{\mathrm{B}}T$ (where $T = 298K$ is the room temperature and k_{B} is Boltzmann's constant) which leads to $A_{\mathrm{NN}} = 15.8\,k_{\mathrm{B}}T$ and $A_{\mathrm{Nm}} = 16.7\,k_{\mathrm{B}}T$. Additional details about the simulation systems are given in Table S2.

All our MD simulations are performed in the NVT ensemble using the HOOMD-blue

Table S2: Information about the simulation systems.

Sample ID	Grafting density $[a^{-2}]$	Number of grafting points at $R = 10a$	Number of NPs	Number of monomers per chain	Total number of particles in the system	Box length $[a]$
DP100	0.61	766	100	7	536300	102.42
DP1170	0.08	100	100	61	610100	104.32
DP530	0.30	376	50	28	526450	93.72
DP1300	0.53	666	20	68	905780	104.37

software package.[11–13] Periodic boundary conditions are applied along the x, y and z directions. The temperature of the system is kept constant at $T = 1.0\varepsilon/k_B$ using a Langevin thermostat. We set the simulation time step to $\Delta t = 0.002\tau$, where $\tau = \sqrt{ma^2/(k_\mathrm{B}T)}$ is the unit of time. Initially, all grafted NPs are placed randomly in a cubic box that is sufficiently large to avoid any overlap between grafted chains of different NPs. At this stage, the monomer-monomer interactions are set to purely repulsive by truncating U_mm at $r_\mathrm{c,mm} = 2^{1/6}a$. Then the simulation box is gradually shrunken over 5×10^6 MD steps until the desired monomer density ρ is reached. The system is then simulated for another 5×10^6 MD steps. Finally, the attractive contribution of U_mm is turned on by setting $r_\mathrm{c,mm} = 3a$, and the system is evolved for 2×10^7 time steps. Measurements were taken during the last 4×10^6 steps of this period. Figure S2 shows the pressure, P, the potential energy, E, and the polymer radius of gyration, R_g, during this time. The data have been normalized by their mean values during this period. It clearly visible that all quantities have leveled off, which indicates that equilibrium has been reached. We repeated this procedure for selected state points using different starting configurations and did not observe any significant impact on the final structures and properties.

The bulk modulus is computed using the relation

$$K = -V\frac{\mathrm{d}P}{\mathrm{d}V}. \tag{5}$$

In order to determine the slope $\mathrm{d}P/\mathrm{d}V$, we ran multiple simulations where we isotropically

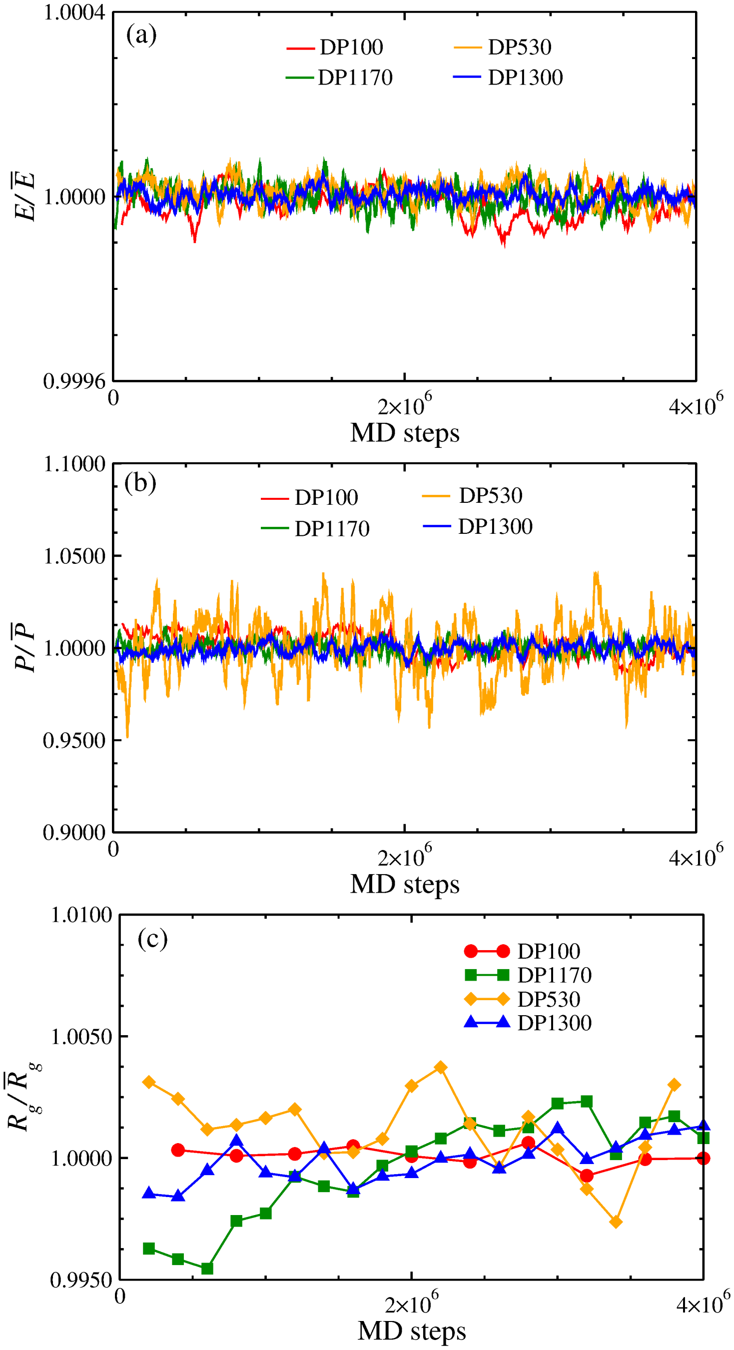

Figure S2: Plot of the normalized (with respect to their mean value) (a) potential energy, E, (b) pressure, P, and (c) radius of gyration, R_g as a function of MD steps. The flat plateaus indicate that all systems have reached equilibrium.

increased and decreased the volume of the simulation box up to 1%. In Fig. S3, we have plotted P versus V. The slope $\mathrm{d}P/\mathrm{d}V$ is shown by the solid lines, which indicate that the systems still are in the linear response regime. All simulation results presented in the main manuscript have been obtained at (reduced) monomer density $\rho = 0.86$, where the systems are still in the liquid regime.[14] The individual contributions from core-core ($K_{\mathrm{c-c}}$), core-polymer ($K_{\mathrm{c-p}}$), and polymer-polymer ($K_{\mathrm{p-p}}$) interactions have been obtained by computing the corresponding contributions to the pressure P and computing its derivative with respect to the system volume V. We validated the self consistency of this approach by verifying the expected equality $K = K_{\mathrm{c-c}} + K_{\mathrm{c-p}} + K_{\mathrm{p-p}}$.

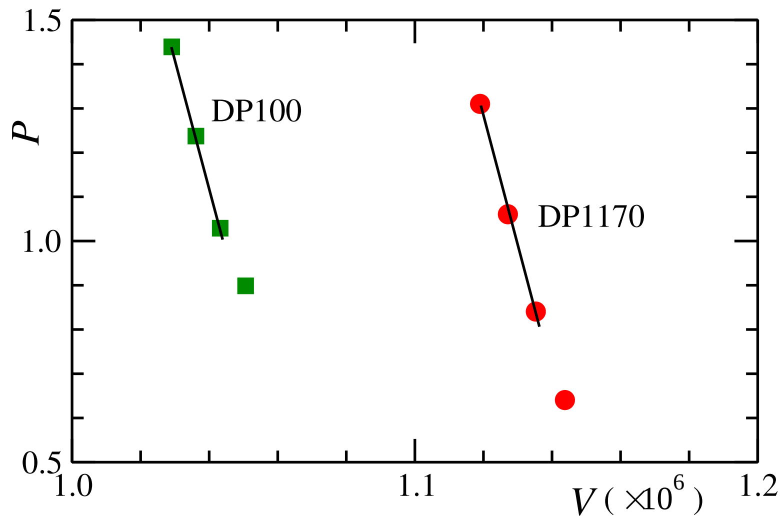

Figure S3: Plot of P versus V at different monomer densities, ρ, for DP100 and DP1170.

Quantification of Brush Overlap: The overlap between the grafted polymers belonging to the same NP and the other NPs is quantified by δ, defined as[15]

$$\delta = \frac{4\pi \left[\int_0^\infty \mathrm{d}r r^2 \rho_{\mathrm{s}}(r)\rho_{\mathrm{o}}(r)\right]^2}{\int_0^\infty \mathrm{d}r r^4 \rho_{\mathrm{s}}^2(r)\rho_{\mathrm{o}}^2(r)} \tag{6}$$

where ρ_{s} is the monomer density of grafted polymers belonging to the same NP and ρ_{o} is the monomer density of polymers belonging to other NPs.

Identification of Single and Double Kinks using Z1 Algorithm: Fig. S4 shows a schematic of different types of kinks formed by the grafted chains which are obtained by using the Z1 algorithm.[16–18] Here, point A represents a single kink, and points B and C represent double kinks. The double kink at point B is formed by the chains belong to the same NP (measure of $\langle Z_s \rangle$), whereas point C demonstrates a double kink formed by the chains coming from two different NPs (measure of $\langle Z_o \rangle$).

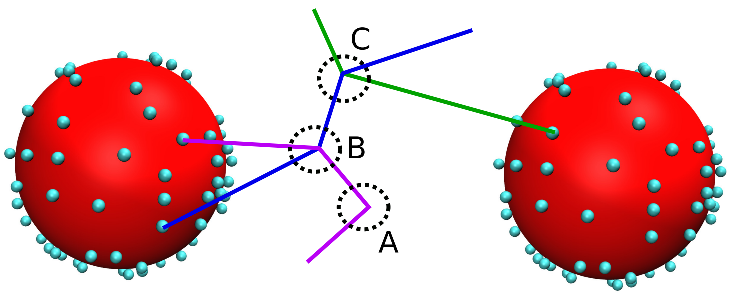

Figure S4: Schematic representation of single and double kinks.

Additional Experimental Results

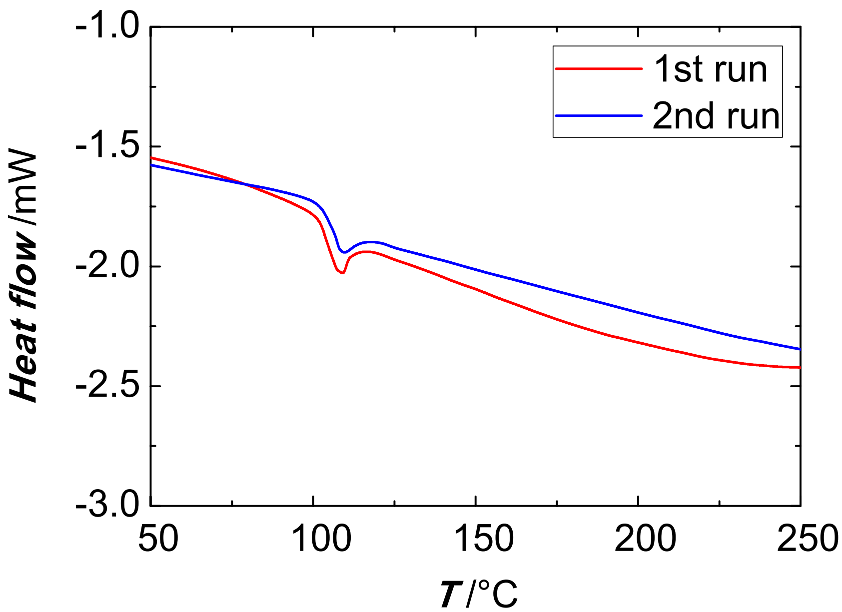

Figure S5: Heat flow of DP530 (PS-grafted SiO_2, $N = 530$ and $\sigma = 0.27\,\mathrm{nm}^{-2}$) on the first and second heating. All heating rates were $10\,\mathrm{K/min}$.) Both DSC traces show only a glass transition implying an amorphous PS matrix.

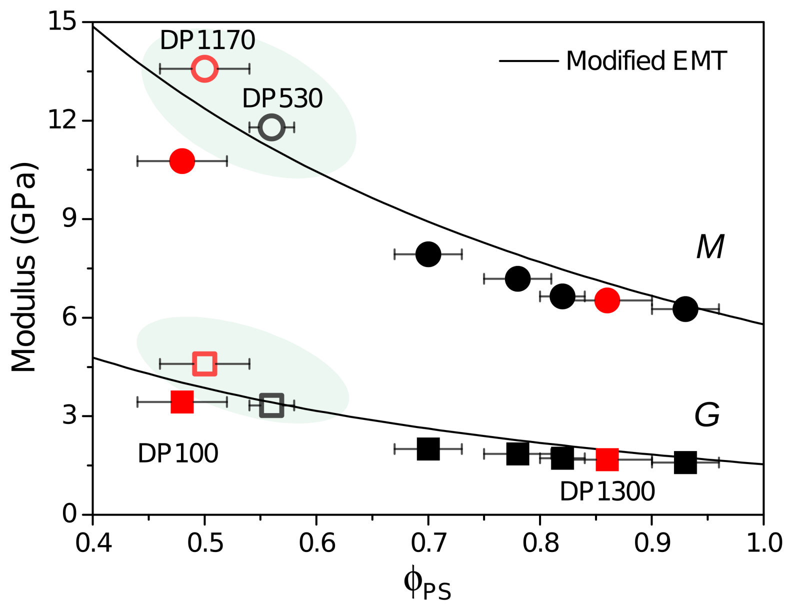

Figure S6: Longitudinal, M, (circles) and shear, G, (squares) elastic moduli for various PS tethered silica films with different PS-volume fraction for densely (solid circles and squares) and sparsely (open circles and squares in the shaded areas) grafted particle systems. The representation by the modified effective medium theory is shown by the solid lines.[19]

Additional Simulation Results

Bond autocorrelation function: To quantify the dynamics of the grafted chains we computed the bond autocorrelation function $A(\Delta t) = \langle \mathbf{b}(t)\mathbf{b}(t_0)\rangle$, with translated time $\Delta t = t - t_0$. The data for the NP systems as well as for the bulk polymer systems is presented in Fig. S7 as a function of Δt. For the pure polymer systems, $A(\Delta t)$ decays quickly to zero, with a slower decay for the longer chains, as expected. For the grafted systems, however, the bond autocorrelation function exhibits a much slower decay and a non-monotonic chain length dependence. This slowing down originates from the constrained degrees of freedom of the grafted chains, which disallow free rotation of the bonds near the NP core. This effect becomes less pronounced for longer polymers, since a smaller fraction of bonds is at the core surface. Another reason for the slower decay of $A(\Delta t)$ is the chain stretching occurring at high grafting densities, which further reduces the monomer mobility: for example, $A(\Delta t)$ for DP530 (intermediate grafting density) decays slower than $A(\Delta t)$ for DP1170 (low grafting density), although the grafted chains of DP530 are considerably shorter than of DP1170.

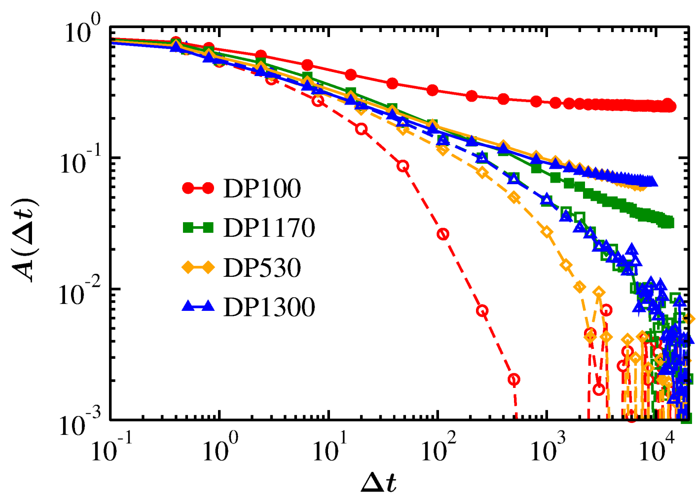

Figure S7: Plot of the bond autocorrelation function, $A(\Delta t)$, as a function of the translated time Δt, on a log-log scale. Solid symbols show results for grafted systems, while open symbols with the same color represent their corresponding bulk systems.

Persistence length: The persistence length ℓ_p is calculated using the relation

$$\ell_p = -\frac{b}{\ln\langle cos\Theta_{ijk}\rangle} \tag{7}$$

where b is the average bond length and Θ_{ijk} is the angle between two consecutive bond vectors $\mathbf{b}_{ij}$ and $\mathbf{b}_{jk}$ connecting monomers i, j and j, k, respectively. The monomers (and bonds) are numbered in an ascending order starting from the grafting point.

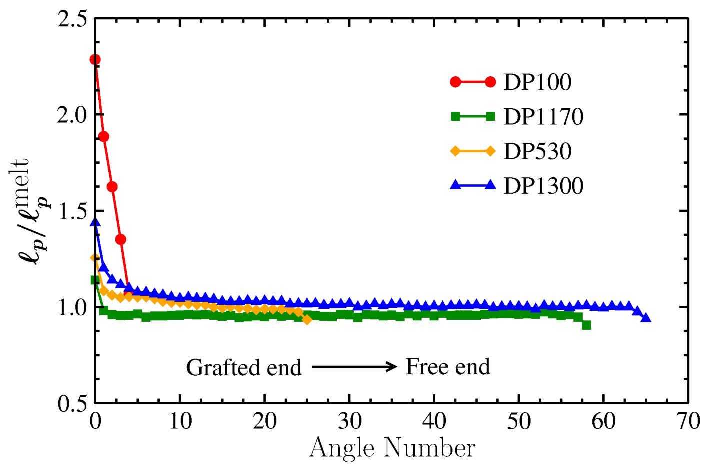

Figure S8: Plot of persistence length, ℓ_p, normalized by the persistence length in the pure melt ℓ_p^{melt} as a function of bond number from the surface of the NP.

Coarse-Grained Model and its Treatment based on Integral Equation Theory: The high-frequency shear modulus is computed using the Zwanzig-Mountain relation[20]

$$G_\infty = \frac{K_\mathrm{B}T}{R^3}\left(\frac{3\phi_\mathrm{c}}{4\pi} + \frac{3\phi_\mathrm{c}^2}{40\pi}\int_0^\infty g(r)\left[k_\mathrm{B}Tr^4\frac{\mathrm{d}U(r)}{\mathrm{d}r}\right]\mathrm{d}r\right) \tag{8}$$

where $\phi_\mathrm{c} = 1 - \phi_\mathrm{PS}$ is the effective packing fraction of the hard NP core, $U(r)$ is the effective potential between brush-coated spherical NPs, and $g(r)$ is the corresponding radial distribution function. In this work, we employed the model developed by Rabani et al.,[21,22] where the NP consists of a rigid core with radius R surrounded by a spherical polymer shell of thickness h (see Fig. S9). The effective interaction potential between NPs, $U(r)$, can be estimated assuming uniform filling of the polymer shell with monomers of the grafted chains, which interact via the LJ potential.[21,22] The corresponding $g(r)$ can be calculated from the non-local integral equation theory with hypernetted-chain closure.[21,22] Taking the values for ϕ_c, h, and d from experiments, we can use eq. (8) to compute G_∞.

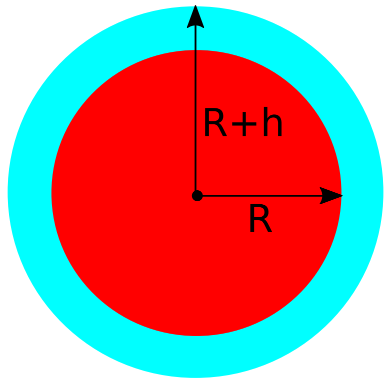

Figure S9: Schematic representation of the model of Rabani et al. The red region represents the hard core of the NP and the cyan area represents the soft polymer corona.

References

(1) Hui, C. M.; Pietrasik, J.; Schmitt, M.; Mahoney, C.; Choi, J.; Bockstaller, M. R.; Matyjaszewski, K. Surface-Initiated Polymerization as an Enabling Tool for Multifunctional (Nano-)Engineered Hybrid Materials. *Chem. Mater.* **2014**, *26*, 745–762.

(2) Cang, Y.; Reuss, A. N.; Lee, J.; Yan, J.; Zhang, J.; Alonso-Redondo, E.; Sainidou, R.; Rembert, P.; Matyjaszewski, K.; Bockstaller, M. R.; Fytas, G. Thermomechanical Properties and Glass Dynamics of Polymer-Tethered Colloidal Particles and Films. *Macromolecules* **2017**, *50*, 8658–8669.

(3) Zhao, D.; Schneider, D.; Fytas, G.; Kumar, S. K. Controlling the Thermomechanical Behavior of Nanoparticle/Polymer Films. *ACS Nano* **2014**, *8*, 8163–8173.

(4) Hamaker, H. C. The London-van der Waals attraction between spherical particles. *Physica* **1937**, *4*, 1058–1072.

(5) Cheng, S.; Grest, G. S. Structure and Diffusion of Nanoparticle Monolayers Floating at Liquid/Vapor Interfaces: A Molecular Dynamics Study. *J. Chem. Phys.* **2012**, *136*, 214702.

(6) Frenkel, D.; Smit, B. *Understanding Molecular Simulations: From Algorithm to Applications*; Academic Press: San Diego, 2002.

(7) Kremer, K.; Grest, G. S. Dynamics of Entangled Linear Polymer Melts: A Molecular-Dynamics Simulation. *J. Chem. Phys.* **1990**, *92*, 5057–5086.

(8) Grest, G. S.; Kremer, K. Molecular Dynamics Simulation for Polymers in the Presence of a Heat Bath. *Phys. Rev. A* **1986**, *33*, 3628–3631.

(9) Hiemenz, P. C.; Lodge, T. *Polymer Chemistry*; CRC Press: London, 2007.

(10) Israelachvili, J. N. *Intermolecular and Surface Forces*; Academic Press: USA, 2011.

(11) Anderson, J. A.; Lorenz, C. D.; Travesset, A. General Purpose Molecular Dynamics Simulations Fully Implemented on Graphics Processing Units. *J. Comput. Phys.* **2008**, *227*, 5342 – 5359.

(12) Glaser, J.; Nguyen, T. D.; Anderson, J. A.; Lui, P.; Spiga, F.; Millan, J. A.; Morse, D. C.; Glotzer, S. C. Strong Scaling of General-Purpose Molecular Dynamics Simulations on GPUs. *Comput. Phys. Commun.* **2015**, *192*, 97 – 107.

(13) Howard, M. P.; Anderson, J. A.; Nikoubashman, A.; Glotzer, S. C.; Panagiotopoulos, A. Z. Efficient Neighbor List Calculation for Molecular Simulation of Colloidal Systems Using Graphics Processing Units. *Comput. Phys. Commun.* **2016**, *203*, 45 – 52.

(14) Hansen, J.-P.; Verlet, L. Phase Transitions of the Lennard-Jones System. *Phys. Rev.* **1969**, *184*, 151 – 161.

(15) Egorov, S. A.; Binder, K. Effect of Solvent Quality on the Dispersibility of Polymer-Grafted Spherical Nanoparticles in Polymer Solutions. *J. Chem. Phys.* **2012**, *137*, 094901.

(16) Kröger, M. Shortest Multiple Disconnected Path for the Analysis of Entanglements in Two- and Three-Dimensional Polymeric Systems. *Comput. Phys. Commun.* **2005**, *168*, 209–232.

(17) Karayiannis, N. C.; Kröger, M. Combined Molecular Algorithms for the Generation, Equilibration and Topological Analysis of Entangled Polymers: Methodology and Performance. *Int. J. Mol. Sci.* **2009**, *10*, 5054–5089.

(18) Jiao, Y.; Tibbits, A.; Gillman, A.; Hsiao, M.-S.; Buskohl, P.; Drummy, L. F.; Vaia, R. A. Deformation Behavior of Polystyrene-Grafted Nanoparticle Assemblies with Low Grafting Density. *Macromolecules* **2018**, *51*, 7257–7265.

(19) Gaunaurd, G. C.; Wertman, W. Comparison of Effective Medium Theories for Inhomogeneous Continua. *J. Acoust. Soc. Am.* **1989**, *85*, 541–554.

(20) Zwanzig, R.; Mountain, R. D. High-Frequency Elastic Moduli of Simple Fluids. *J. Chem. Phys.* **1965**, *43*, 4464–4471.

(21) Rabani, E.; Egorov, S. A. Interactions Between Passivated Nanoparticles in Solutions: Beyond the Continuum Model. *J. Chem. Phys.* **2001**, *115*, 3437–3440.

(22) Rabani, E.; Egorov, S. A. Integral Equation Theory for the Interactions between Passivated Nanocrystals in Supercritical Fluids: Solvophobic and Solvophilic Cases. *J. Phys. Chem. B* **2002**, *106*, 6771–6778.